Scanning Tunneling Microscopy: *A Tool for Studying Self-Assembly and Model Systems for Molecular Devices*

By: Thomas Müller

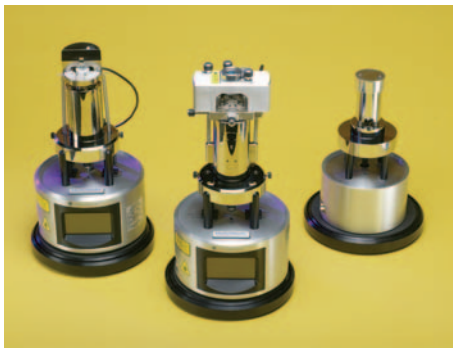

Figure 1. Scanning tunneling microscopy options available from Veeco Instruments with the Digital Instruments NanoScope® series of controllers. Displayed are the MS-10 stand-alone STM base (right), and the versatile MultiMode® SPM, with STM tipview adapter, (left). In addition, a low current accessory is available for the MultiMode SPM and an STM adapter for the Dimension 3100 SPM (not shown).

Introduction

The invention of the scanning tunneling microscope in 1982[1-3] initiated the creation of what is known today as a whole family of scanning probe microscopies (SPMs). The importance of scanning tunneling microscopy (STM) was soon recognized and culminated in the award of half the 1986 Nobel Prize in Physics to Binnig and Rohrer. Early STM work focused mainly on the clean, bare surfaces that exist under ultrahigh vacuum (UHV) conditions[2-4] and provide ideal systems for formulating and testing theories of tip-sample interactions and electron transport.[5,6] A great expansion of STM research was started in 1986, when Digital Instruments introduced the first commercial scanning tunneling microscope operating in ambient conditions, the NanoScope STM.

The ability to perform STM work in air, under solutions, and within electrochemical cells has made the interrogation of self-assembly practical. The high resolution achieved with relative ease in STM images sets this technique apart from other SPMs and has allowed numerous STM studies to address the structure and dynamics of self-assembled monolayers in exquisite detail.[7-9] Two-dimensional self-assembly on surfaces and at interfaces is often cited as an important ingredient for any future nanoscale engineering. The same can be said for single-molecule devices. Indeed, the understanding and control of charge transport in model systems for such molecular devices constitutes an important focal point of current efforts in nanoscience. Due to its ability to interrogate electron transport with submolecular resolution, STM is uniquely positioned as an important tool in this area. Recent years have witnessed a synthesis where ambient STM studies have been designed to interrogate charge transport in molecular devices while building on previous work to self-assemble the species of interest into ordered arrays.

Several options are available from Veeco Instruments for performing STM with the NanoScope series of controllers (see Figure 1). As proven in numerous publications, high-resolution STM imaging is achieved routinely with both, the cost-effective MS-10 stand-alone STM base as well as the versatile MultiMode SPM with STM converter. For applications demanding detection of extremely small (sub-pA) tunneling currents, a low-current accessory with switchable bandwidth and gains is available for the MultiMode. An STM tip holder is also available for the Dimension series of microscopes, allowing for STM measurements on large samples.

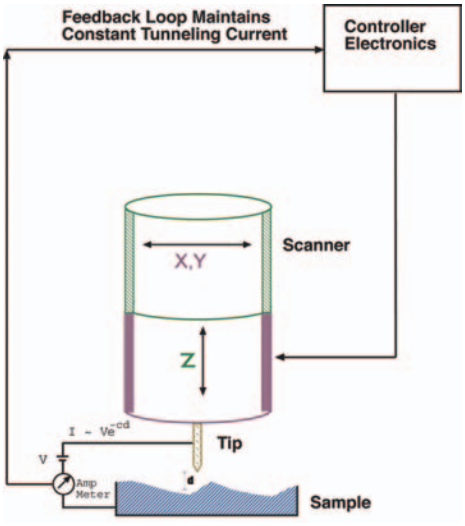

Figure 2. Schematic view of the basic configuration for scanning tunneling microscopy.

Operating Principle and Implications

Basic Setup and Modes

Like other types of scanning probe microscopes, scanning tunneling microscopes contain a sharp probe that is scanned relative to a sample surface using precisely controlled voltages applied to piezoelectric elements while the motion of the tip (or sample) normal to the sample surface is controlled by a feedback loop (see Figure 2). What sets STM apart from other SPMs is the use of the tunneling current between tip and sample as error signal for that feedback loop. While this limits STM studies to conductive substrates, the steep exponential distance dependence of the tunneling current allows for spatial resolution rarely achieved in other SPM modes. Typical bias voltages vary from millivolts for bare metal or graphite surfaces to 1-2 volts for semiconductor substrates and molecular adsorbates. Tunneling currents are usually in the pico-ampere to nano-ampere range. As no force measurement is taking place, the STM probe is not attached to a cantilever. Instead, the probe is the atomically-sharp tip of a metal wire. Typically, either mechanically formed Pt/Ir-tips or electrochemically etched Pt/Ir or W-tips are employed.

As with all SPMs, the probe (here the STM tip) can be made to follow the sample topography in detail. In that case scan rates (in lines per time unit) and feedback parameters employed tend to be of the same order of magnitude as for AFM. However, in STM the topography is defined by a constant tunneling current (at the given voltage bias), thus this mode of operation is referred to as constant current mode.

Alternatively, the feedback parameters can be reduced and the scan rates increased drastically, so that the tip (or sample) moves at approximately constant height ("constant height mode"). Instead of the height, the error signal (i.e., tunneling current) is being recorded. The relatively flat samples often interrogated in ambient STM studies are conducive to this mode of operation, with the higher scan rates helping to reduce the influence of thermal and mechanical drift, which can be important due to the small (often <100nm) scan sizes. However, due to their more well-defined tip-sample separation, STM topographs acquired in constant current mode may be preferable for comparisons with theoretical predictions.

In analogy to other SPMs the imaging capability of STM is complemented by a type of single-point spectroscopy (SPS), here also referred to as scanning tunneling spectroscopy (STS). In this mode, the current is recorded at a given location of the sample as a function of another parameter, typically the bias voltage or tip-sample separation.

Source of Image Contrast

In constant current mode the sample topography displayed in an STM image is defined by a constant tunneling current between tip and sample at the chosen bias voltage. The interpretation of such "topography" in terms of sample properties is at first less straightforward than in the case of AFM, where the

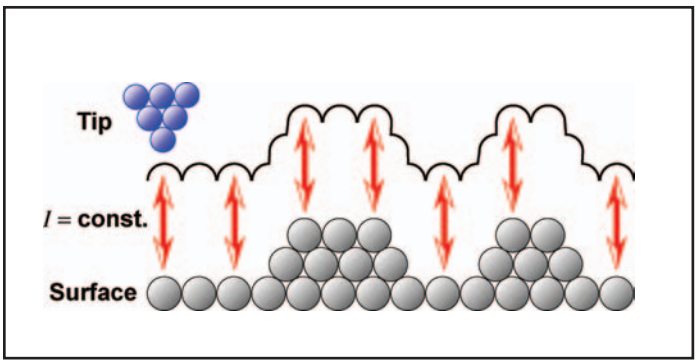

Figure 3. Imaging a surface in constant current mode. The surface topography is defined by a constant tunneling current.

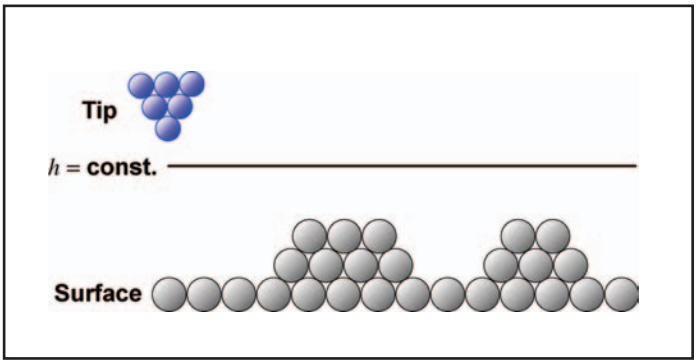

Figure 4. Imaging a surface in constant height mode. The error signal (i.e., tunneling current) is being recorded.

probe moves such as to press on the sample with constant force. As shown by Tersoff and Hamann, the tunneling current between a metallic tip and a metallic surface is proportional to the surface local density of states (LDOS) at the Fermi level, E_F, evaluated at the location of the tip.[5,6] While this simple result is subject to certain approximations, such as small bias, low temperature, and a spherical tip represented solely by an *s*-wave function, the interpretation of STM images in terms of the surface LDOS at (or near) E_F has met with overwhelming success.

The present application note is mainly concerned with surfaces decorated with relatively weakly interacting molecules. In contrast to the assumptions underlying Tersoff and Hamann's theory, larger bias voltages (typically on the order of 1V) and higher temperatures (usually approximately room temperature) are employed for imaging such systems, thus expanding somewhat the energy range of surface states involved in tunneling. In addition, when considering the density of states of the overall system, the molecular orbitals associated with the adsorbate must be taken into account[7,10,11] as illustrated in Figure 5.

In constructing a diagram as shown schematically in Figure 5, the energies of the adsorbate states need to be placed with respect to the energies of the substrate surface states. Shown in Figure 5 are the frontier orbitals of the molecular adsorbate, i.e., the highest occupied molecular orbital, HOMO, and the lowest unoccupied molecular orbital, LUMO. As a first approximation, the vacuum levels can be "pinned" or "lined up", as a free electron does not care where it came from. As indicated in Figure 5, the Fermi level of the substrate and the HOMO of a free molecule are referred to the vacuum level by the workfunction, ϕ, and ionization potential, *IP*,

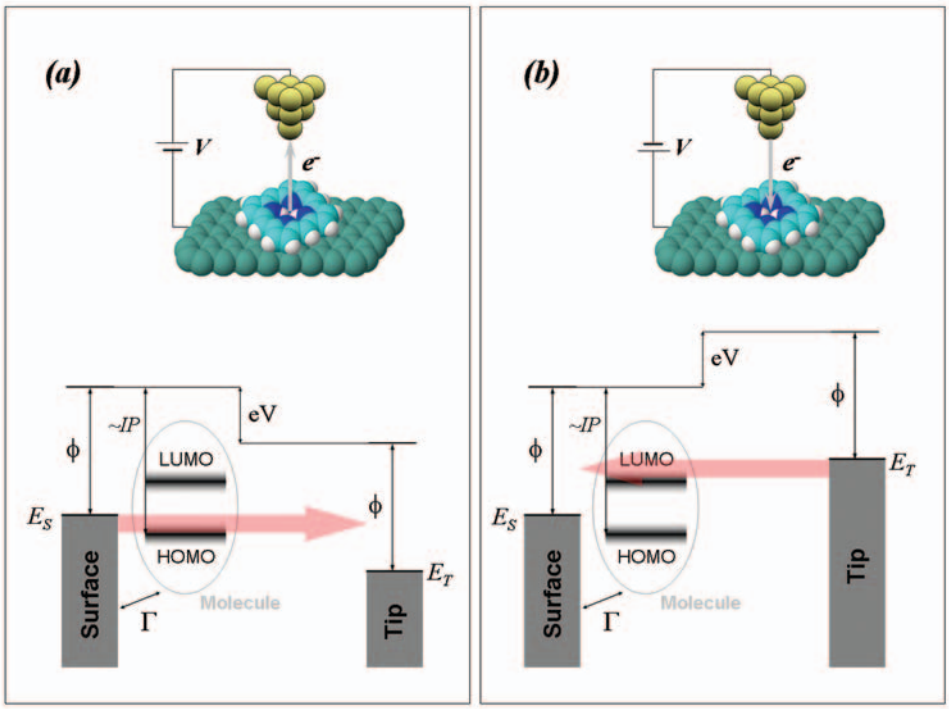

Figure 5. Energy diagram for an STM junction when applying a negative (a) or positive (b) sample bias. The position of molecular frontier orbitals (HOMO and LUMO) and Fermi levels of substrate (E_S) and tip (E_T) are indicated. While molecular energy levels are broadened and shifted due to electronic coupling (Γ) to substrate states (and other phenomena), their approximate position can be estimated by pinning the vacuum level of the isolated molecule to that of the substrate.

respectively. However, a quantitative treatment will have to take into account shifts (and broadening) of energy levels due to effects such as the electronic coupling, Γ, between adsorbate and substrate states, the presence of any solvent (typically lowering the energy of ions), and the electric field in the vicinity of the STM tip (typically ~10^7 V/cm).

At first it may seem that the adsorbate does not contribute a significant number of states to the overall system, especially not near the Fermi level. In the case of Xe on Ni, not a single adsorbate state lies within several eV of the Fermi level. Nevertheless, Xe atoms on Ni have been imaged successfully.[12] The presence of Xe has a significant influence on the LDOS near the Fermi level as evaluated at the position of the STM tip. Simply due to its spatial location even this most insulating adsorbate can serve as "antenna" (*i.e.*, at least a better antenna than vacuum) for the transport of electrons across the tunneling junction. Thus, STM images of insulating adsorbates can provide a topographic map of the topmost adsorbate atoms.[13]

When the surface adsorbate exhibits electronic states near the Fermi level (i.e., for a moderate HOMO-LUMO gap), then individual molecular orbitals may dominate in the mediation of the electron transmission. For negative sample bias, electrons from filled surface states tunnel to the tip. As illustrated in Figure 5a, mediation of this process is dominated by the HOMO of the adsorbate, if the HOMO is situated near the Fermi level. Conversely, electrons tunnel into empty surface states for positive sample bias. As illustrated in Figure 5b, the LUMO may

play a dominant role in this case if it is located near the Fermi level. Thus, with appropriately chosen bias voltages STM images can reveal the shape of individual molecular orbitals.

The energy diagram shown in Figure 5 not only applies for adsorbate species in an STM tunneling junction. Essentially the same diagram is used in the analysis of single-molecule device studies performed with break junctions and electromigration junctions. The only difference is the assumption of significant electronic coupling to both electrodes in those cases. Therefore, the schematic diagram shown in Figure 5 not only explains why essentially insulating adsorbate molecules can be imaged with STM but also illustrates how STM and STS provide information relevant to molecular device properties. STM and STS data for appropriately chosen systems can intrinsically provide information about the mediation of charge transport by individual molecular states of single molecules.

In the above treatment the adsorbed molecule is being considered solely as an object with an electronic structure that plays a role in mediating the electron tunneling by changing the overall LDOS of the decorated surface. In general, molecules exhibit additional degrees of freedom (vibrations, rotations, translations). The associated dynamics need to be considered for the interpretation of STM and STS data for several reasons. First, large-scale nuclear motion entails a corresponding spatial redistribution of electron density that can affect the tunneling probability.[7,14] Second, vibrational and rotational degrees of freedom are associated with spectral fine structure. In experiments performed at or near room temperature (the focus of this application note), thermal broadening reduces the energy resolution of tunneling spectra sufficiently to prevent detection of such fine structure. However, this is not the case in UHV STM experiments performed a few degrees above absolute zero where vibrational structure has been observed due to its influence on both, the elastic and inelastic tunneling probability.[15]

Application Examples

2-D Self-Assembly: Chemisorbed and Physisorbed Systems

The study of two-dimensional self-assembly on surfaces and at interfaces is motivated by many practical applications ranging from lubrication and catalysis to the role envisioned for self-assembly in future nanoscale engineering. Several types of self-assembling systems have received considerable interest, including thiols chemisorbed on Au(111)[9] and alkane derivatives physisorbed on the basal plane of graphite.[7] The chemisorption of thiols on gold is an irreversible process driven by the formation of the strong Au-S bond. Intermolecular interactions and the structure of the Au(111) surface also play a role during the self-assembly. Dense monolayers are formed, where only the thiol headgroup is in contact with the gold surface. In the case of alkane thiols, a commensurate ($\sqrt{3} \times \sqrt{3}$)R30° overlayer structure is formed with additional superstructures depending on chain length and functionalization.

Figure 6 shows an example of an ambient high-resolution STM image where the ordered structure of a thiol layer can be seen clearly.[16] The monolayer was prepared by exposing a gold substrate to an ethanol solution. Both molecular species of interest were incorporated in the monolayer and can be distinguished in the STM image. Thus, model systems for nanoscience can be embedded in a sea of simple alkane thiols and studied by STM.

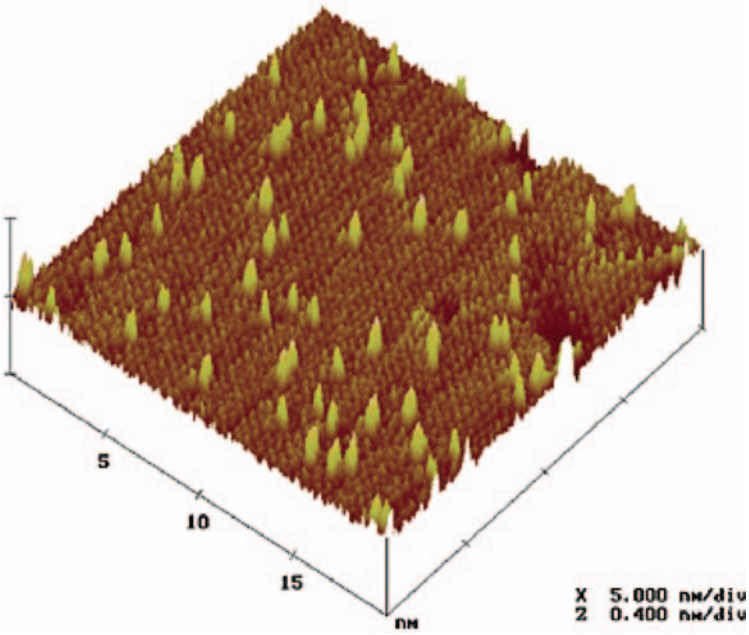

Figure 6. Low-current STM topographic images of mixed self-assembled monolayers on Au(111) formed from a solution of 11-mercaptoundecanoic acid and decanethiol (1:9) at 65°C with a bias voltage of 1.02 V and a set point current of 1.10 pA. Reprinted in part with permission from Lingyan Li, Shengfu Chen, and Shaoyi Jiang, Langmuir 2003, 19 (8), 3266 -3271. © (2003) American Chemical Society.

Alkane thiols are subject to oxidation in air and high-resolution STM studies are often performed in UHV, even when the preparation takes place by immersing the substrate in a solution. The present application note is mainly concerned with physisorbed monolayers self-assembled on the basal plane of graphite, which are frequently generated and probed in ambient conditions at the liquid/solid interface. In contrast to thiols on gold, physisorbed monolayers on graphite are not based on the irreversible formation of a chemical bond between a surface atom and a specific adsorbate functional group. Numerous types of organic molecules permit the formation of weakly-adsorbed monolayers on graphite that exist in equilibrium with a supernatant solution. Often, either long alkyl chains or functional groups (or both) are present with both the associated intermolecular and molecule-substrate interactions providing key driving forces for the self-assembly process. The following sections of this application note will provide several examples for STM work on such self-assembled systems, including molecules that were custom-tailored to exhibit both, the desired self-assembly and the molecular device properties of interest.

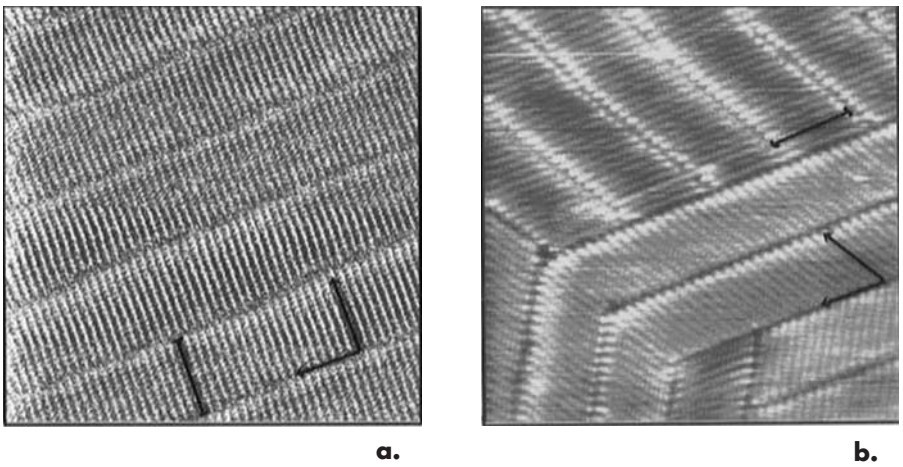

Figure 7. (a) Constant height STM image (20nm × 20nm, sample bias −1.235V, 166pA tunneling current) of triacontane ($C_{30}H_{62}$) in phenyloctane physisorbed on graphite. One molecular length is represented by a black bar. The molecules are oriented with a 90° angle between the molecular axis and the direction of the lamellae. (b) Constant current STM image (20nm x 20nm, sample bias −1.4V, 80pA tunneling current) of triacontanol ($CH_3(CH_2)_{29}OH$) in phenyloctane physisorbed on graphite. One molecular length is indicated by a black bar. The molecules are oriented with a 60° angle between the molecular axis and the direction of the lamellae as indicated on the image. Reprinted in part with permission from Donna M. Cyr, Bhawani Venkataraman, and George W. Flynn, J. Phys. Chem. 1996, 100(32), 13747-59. Copyright (1996) American Chemical Society.

Driving Forces for Self-Assembly on Graphite

Among the first STM studies of self-assembly from solution were those of the monolayers formed by alkanes and their derivatives on graphite.[7,13,17] As can be seen in Figures 7-14, close-packed lamellar structures are formed where the lamellae are composed of parallel alkyl chains each assuming an extended, all-trans conformation. In contrast to the dense self-assembled monolayers formed by alkane thiols on gold substrates,[9] the backbone axis of each molecule is oriented parallel to the plane defined by the substrate surface, thus bringing the entire alkyl chain into contact with the graphite substrate. Dispersion interactions with both, the substrate and neighboring molecules play an important role in the formation of this structure. In the case of alkanes a right angle is formed by the backbone and lamella axes (see Figure 7a), while the introduction of terminal functional groups can lead to different lamella-backbone angles (see Figure 7b).[7] Alkane functionalization affects such structural parameters as the lamella-backbone angle as functional group interactions can exhibit a pronounced angular dependence (in addition to steric requirements) compared to the more isotropic alkane-alkane and alkane-graphite dispersion forces.

The presence of functional groups has effects on the self-assembly that are more subtle than changing the lamella-backbone angle. Note that some of these STM images (*e.g.*, see Figures 8 and 9) clearly reveal the position of individual hydrogen atoms associated with the methylene groups of the carbon backbone. The orientation of individual methylene groups and thus of the whole carbon skeleton with respect to the surface plane can be determined. As shown in Figure 8, alkanes can exhibit different spot patterns, even in successively acquired STM images. Apparently, the plane formed by the all-trans carbon backbone can assume a variety of angles with respect to the substrate surface plane.[13,17] The distribution of angles is influenced by temperature and the presence of solvent.[18,19]

In contrast, a well-defined backbone plane rotation angle is found for alkanoic acids. Figure 9 clearly reveals the zig-zag spot pattern characteristic of the topmost hydrogen atoms when the molecular backbone plane is parallel to the surface plane. Alkanoic acids form hydrogen-bonded dimers. The bulky, hydrogen-bonded acid headgroups force the backbone into the "flat" orientation.

Even more subtle effects follow. The lateral spacing (within lamellae) of alkanes and their derivatives can be expected to depend on the rotation angle around the backbone axis. In bulk alkane crystals, nearest neighbor distances of 4.2Å and 4.8Å are found perpendicular and parallel, respectively, to the planes formed by the carbon skeletons. Ambient STM images suggest that nonfunctionalized alkanes under solution form a commensurate structure with a lateral spacing of 4.26Å,[17] while a wider, noncommensurate structure is formed by alkanoic acids.

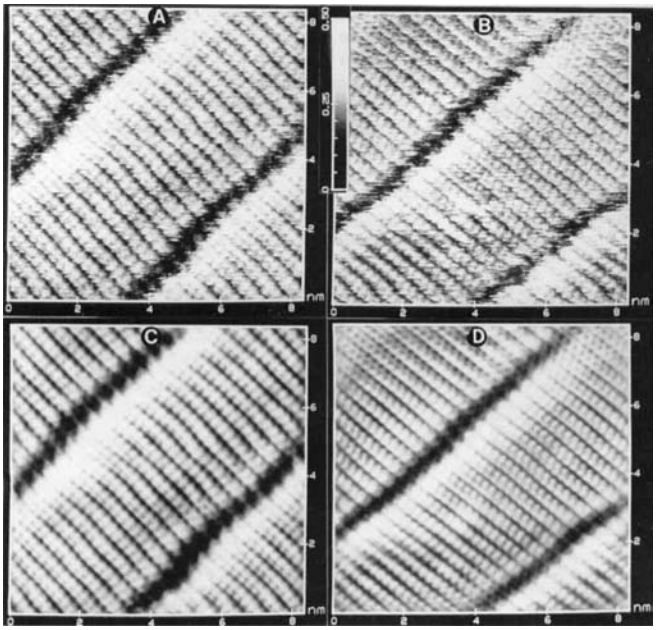

Figure 8. Constant current STM image (sample bias −168mV, 300pA tunneling current) of hexatriacontane at the interface between a dodecane solution and the basal plane of graphite. Panels (a) and (b) show raw data acquired in two successive scans. Panels (c) and (d) show filtered versions of the STM images in (a) and (b), respectively. Used with permission from Weigen Liang, Myung-Hwan Whangbo, Aleksander Wawkuschewski, Hans-Joachim Cantow, and Sergei N. Magonov, Adv. Mater. 1993, 5, 817. Copyright 1993 VCH Verlagsgesellschaft mbH, D-69469 Weinheim.

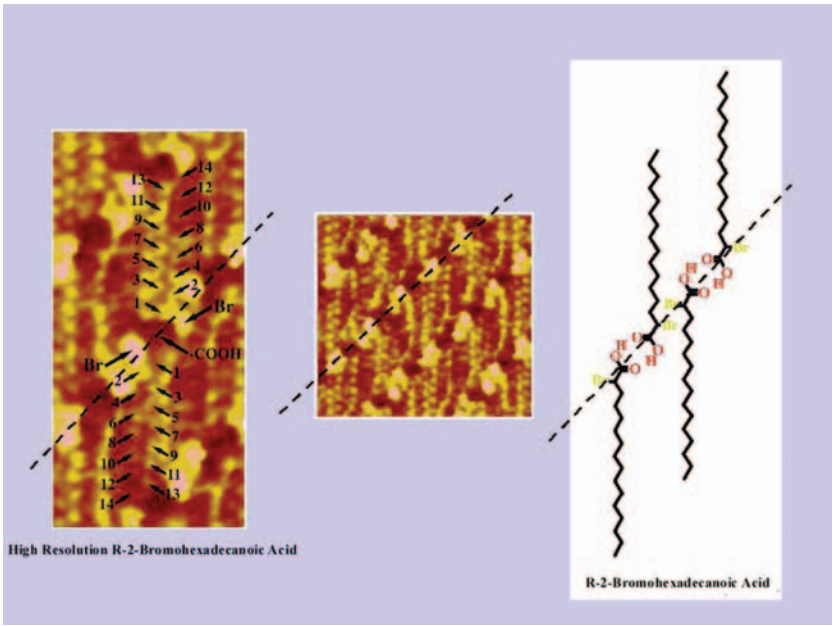

Figure 9. Constant current STM images (-1.4V sample bias, 300 pA tunneling current) and a corresponding model of (*R*)-2-bromohexadecanoic acid in phenyloctane physisorbed on graphite. Numbers and letters in the image refer to individual hydrogen atoms and functional groups while the dashed line emphasizes the 45° angle between lamella and molecular backbone. Reproduced with permission from www.columbia.edu/cu/chemistry/groups/flynn/r2bromo.html.

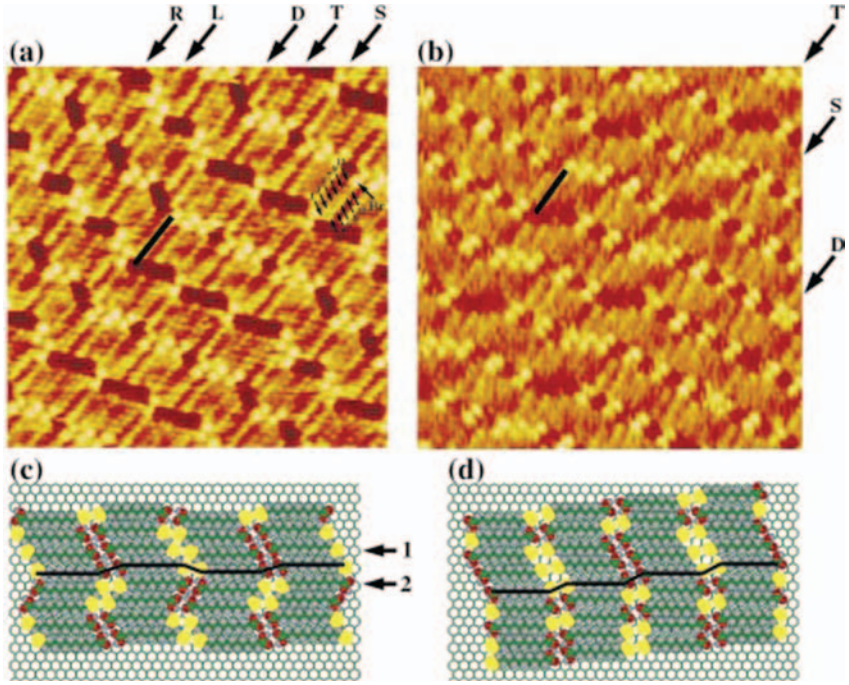

Figure 10. Constant current STM images (12nm×12nm, sample bias −1.4V, 300pA tunneling current) are shown of (a) 12-bromododecanoic acid and (b) 11-bromoundecanoic acid on graphite under phenyloctane solution. Black bars indicate a molecular length. Capital letters S, D, and T point to strips of single, double, and triple-twin structures, respectively. Capital letters R and L point respectively to the positions where the lower twin in a double or triple twin shifts right or left relative to the twin lying above it. The small numbers 1-11 in (a) point to the positions of individual hydrogen and bromine atoms and Br refers to the bromine substituent. (c) and (d) show molecular models for the images displayed in (a) and (b), respectively. Numbers 1 and 2 in (c) refer to rows, where the molecules shift right or left relative to the row above. Reprinted with permission from Hongbin Fang, Leanna C. Giancarlo, and George W. Flynn, J. Phys. Chem. B 1998, 102(38), 7421-4 (1998). Copyright (1998) American Chemical Society.

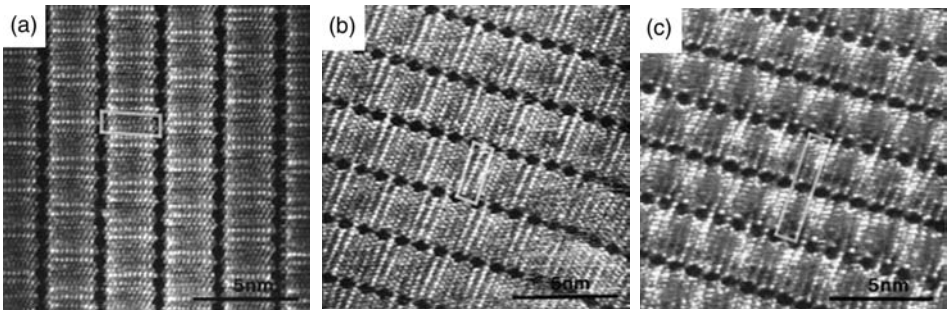

Figure 11. Constant current STM images (~12nm × 12nm, sample bias −1.3V, 800pA tunneling current) are shown of (a,b) behenic acid and (c) nonadecanoic acid on graphite under phenyloctane solution. Unit cells are indicated by parallelograms (a,b) and a rectangle (c). Reprinted with permission from Masahiro Hibino, Akinori Sumi, Hiroshi Tsuchiya, and Ichiro Hatta, J. Phys. Chem. B 1998, 102(23), 4544-7. Copyright (1998) American Chemical Society.

Self-Assembly and Expression of Chirality

The geometric requirement of close-packed monolayer structures allows such seemingly negligible changes as the addition of a single methylene group to a long alkyl chain to alter the self-assembly significantly. Panels a and b of Figure 10 display STM images of 12-bromododecanoic acid and 11-bromoundecanoic acid, respectively.[20] Although only differing by one methylene group, the monolayer structures resulting for these two species are obviously very different. An additional geometric subtlety is associated with the transition from three to two dimensions. The bromoalkanoic acids under consideration are not chiral, *i.e.*, they can be superimposed on their mirror images (assuming free rotation of the terminal bromomethylene group). However, the introduction of the liquid-solid interface removes symmetry elements and prevents free molecular rotation about the carbon backbone axis. As a consequence, two adsorbed states can be distinguished that are mirror images of each other. Alkanoic acids become prochiral upon adsorption on the basal plane of graphite. Close inspection of Figure 10 reveals that in the case of 11-bromoundecanoic acid, immobilization at the interface leads to the formation of chiral (or enantiomorphous) domains, *i.e.*, domains distinct from their mirror image, where all molecules within a domain are of identical "chirality". In contrast, geometric packing requirements lead to the formation of achiral domains for 12-bromoundecanoic acid, where adsorbed molecules of both "chiralities" are present within each domain.[20]

The same effect is known for alkanoic acids without the terminal bromine substituents. In that case, enantiomorphous domains are observed for an even number of carbon atoms (including

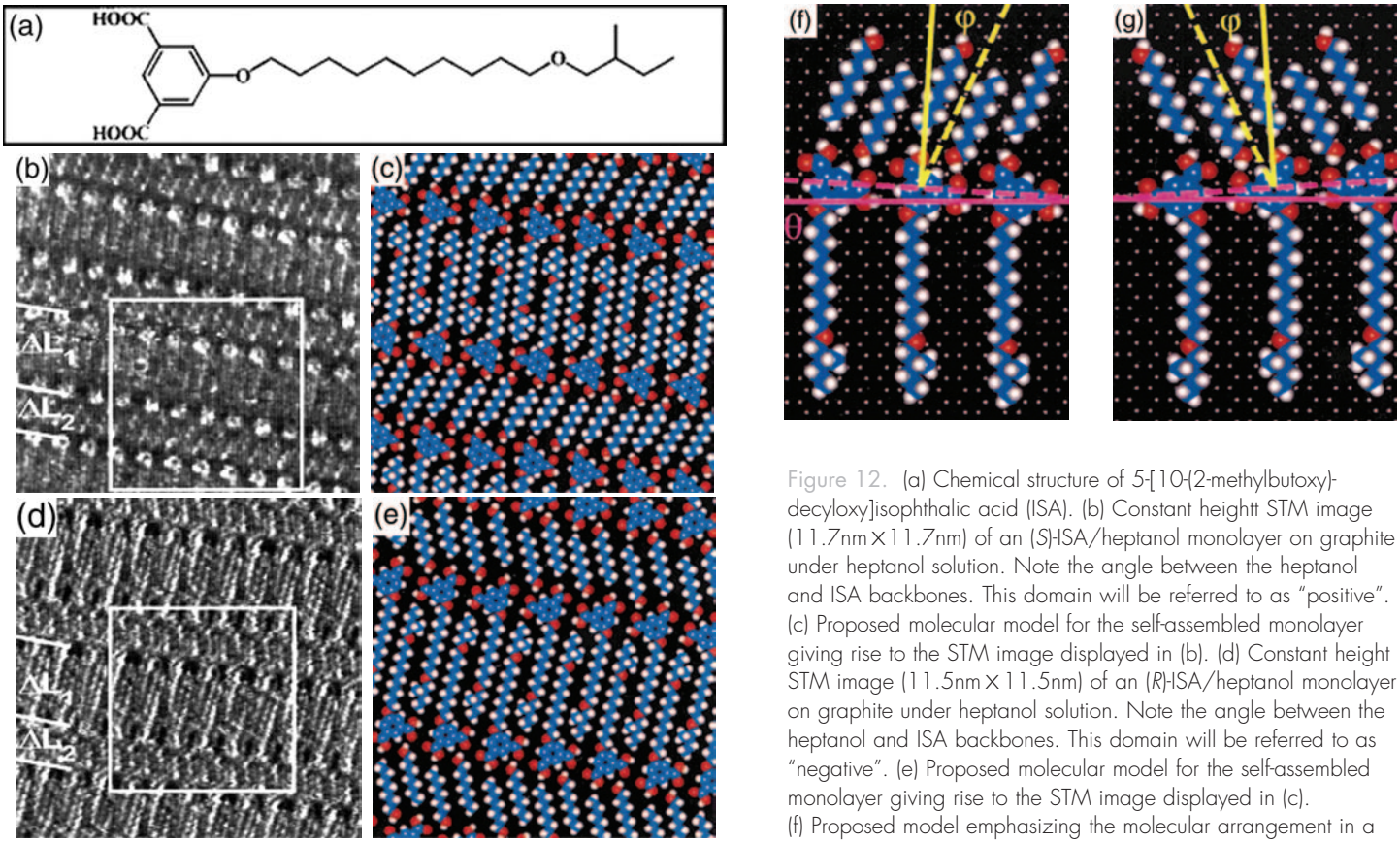

Figure 12. (a) Chemical structure of 5-[10-(2-methylbutoxy)-decyloxy]isophthalic acid (ISA). (b) Constant heightt STM image (11.7nm×11.7nm) of an (*S*)-ISA/heptanol monolayer on graphite under heptanol solution. Note the angle between the heptanol and ISA backbones. This domain will be referred to as "positive". (c) Proposed molecular model for the self-assembled monolayer giving rise to the STM image displayed in (b). (d) Constant height STM image (11.5nm×11.5nm) of an (*R*)-ISA/heptanol monolayer on graphite under heptanol solution. Note the angle between the heptanol and ISA backbones. This domain will be referred to as "negative". (e) Proposed molecular model for the self-assembled monolayer giving rise to the STM image displayed in (c). (f) Proposed model emphasizing the molecular arrangement in a "positive" domain. (g) Proposed model emphasizing the molecular arrangement in a "negative" domain. Reproduced with permission from Steven de Feyter, Petrus C. M. Grim, Markus Rücker, Peter Vanoppen, Christian Meiners, Michel Sieffert, Suresh Valiyaveettil, Klaus Müllen, and Frans C. De Schryver, Angew Chem Int Ed 1998, 37(9), 1223-6. Copyright 1998 Wiley-VCH Verlag GmbH, D-69469 Weinheim.

the acid group).[21] An example of this is shown in Figure 11. Panels (a) and (b) show the two opposite enantiomorphous domains formed by behenic acid ($C_{21}H_{43}COOH$, *i.e.*, with an even number of carbon atoms). The mirror image relationship between the two types of domains is emphasized by the unit cells shown as (non-rectangular) parallelograms. As can be seen in panel (c), nonadecanoic acid (with an odd number of carbon atoms) forms a packing structure with a rectangular unit cell that is identical to its mirror image.

The expression of chirality has also been examined for self-assembled monolayers composed of several distinct molecular building blocks. When mixing chiral with achiral species, the chirality can be not only transferred to the two-dimensional array but also from the chiral to the achiral component. An example of this is shown in Figure 12, where the chiral 5-[10-(2-methylbutoxy)-decyloxy]isophthalic acid (ISA) is self-assembled at the heptanol/graphite interface.[22] Enantiomorphous domains are formed composed of alternating ISA-heptanol lamellae stabilized by hydrogen bonding. The domains are chirally pure not only with respect to ISA but also with respect to the sense of rotation of the HOC bond angle of the coadsorbed heptanol molecules and the angle between the ISA and heptanol molecular backbone axes. The multi-component self-assembly has extended the enantiomorphous character to heptanol.[22] Heptanol has become prochiral.

The opposite effect has also been observed. An achiral solute can form enantiomorphous domains that direct the self-assembly of a chiral cosolute. In that case the template created by the achiral species can afford the resolution of racemic mixtures by separately depositing each enantiomer into chirally pure domains. Exactly this outcome can be seen in Figure 13, where a self-assembled domain of hexadecanoic acid at the phenyloctane-graphite interface is shown, decorated with the chiral (*S*)-2-bromohexadecanoic acid also present in the solution.

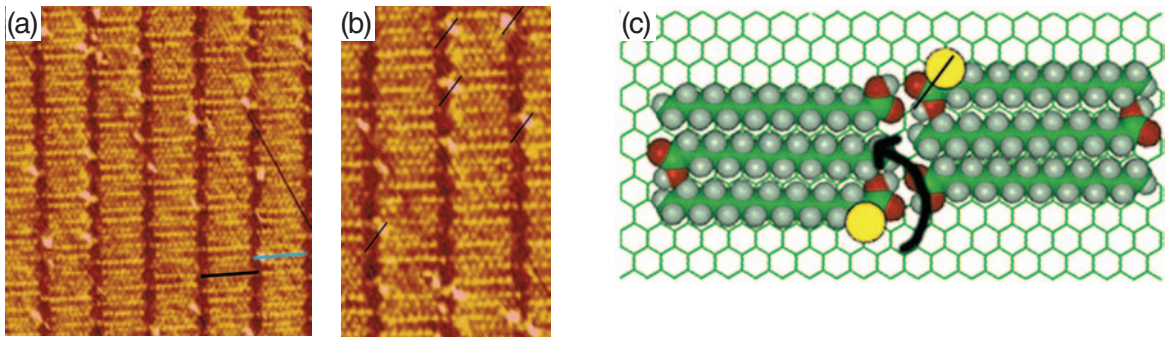

Figure 13. (a) A constant current STM image (13nm×13nm, sample bias −1.5V, 300pA tunneling current) of a domain of hexadecanoic acid interspersed with (*S*)-2-bromohexadecanoic acid is shown where a solid black bar depicts hexadecanoic acid and a blue bar depicts 2-bromohexadecanoic acid. An enlarged portion of (a) is presented in (b) where the bromine atom lies above and to the right or below and to the left of the carboxyl group as highlighted by the superimposed thin black lines. The orientation of the bromine, carboxyl, and alkyl chain on the chiral carbon is used to identify the 2-bromohexadecanoic acid molecules in this domain as the *S* chiral conformers of the molecule. A top view of a model of hexadecanoic acid interspersed by (*S*)-2-bromohexadecanoic acid on the graphite surface is shown in (c). The thin black line superimposed on a bromine/carboxylic combination shows the same pattern depicted in the STM image (b). An arrow demonstrating the counterclockwise direction of the brominecarboxyl group-alkyl group orientation identifies the brominated molecules as the *S* conformer. Reprinted with permission from Dalia G. Yablon, Leanna C. Giancarlo, and George W. Flynn, J. Phys. Chem. B 2000, 104(32), 7627-35. Copyright (2000) American Chemical Society.

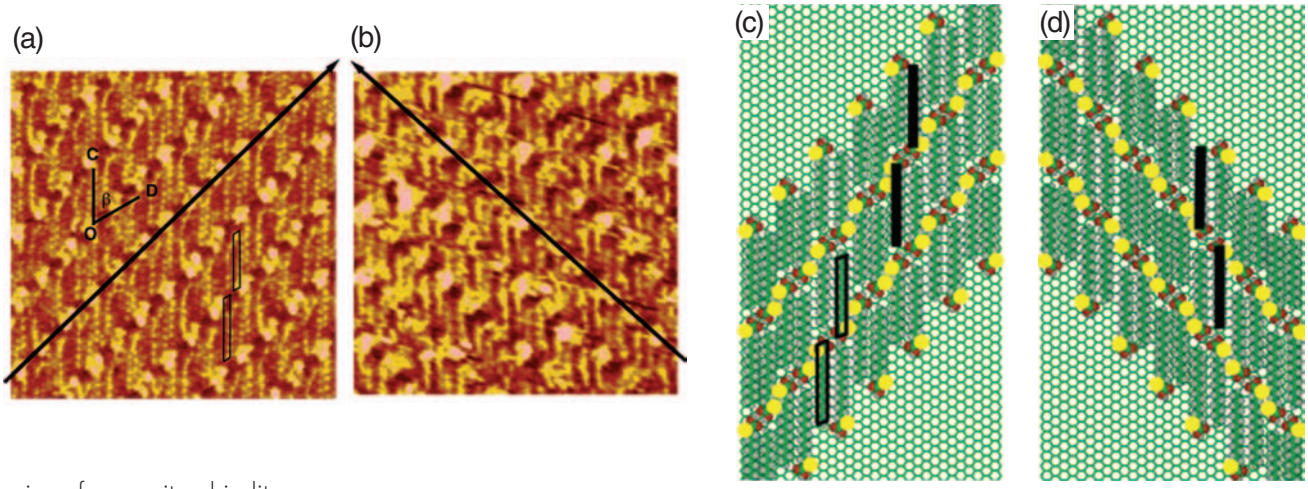

Figure 14. (a) STM topograph of one of the domains formed by the assembly of (*R*)/(*S*)-2-bromohexadecanoic acid on graphite. The "bright" topographic protrusions are assigned as the positions of the α-Br atoms, while the adjacent "dark" topographic depressions correspond to the hydrogen-bonding COOH groups. An alternating pattern of "bright"-"dark"-"bright" runs through the image from lower left to upper right, as denoted by the black arrow. This domain has been assigned as containing *R*-enantiomers exclusively. Two parallelograms denote a hydrogen-bonded molecular pair lying flat on the surface. The angle, formed by the molecular axis, OC, and the direction of the hydrogen-bond, OD, has been measured as 53±5°. (b) A second domain of 2-bromohexadecanoic acid molecules found at the phenyloctane-graphite interface. The alternating "bright"-"dark"-"bright" pattern now extends from lower right to upper left in the topographic image. This domain is the mirror image of that shown in (a) and is comprised only of the *S*-enantiomer. Both (a) and (b) are 12nm×12nm images (-1.4V sample bias, 300 pA tunneling current). (c) A molecular model of (*R*)-2-bromohexadecanoic acid organized on a graphite lattice based on the image shown in (a). The black bars denote a chiral pair of *R-R* molecules bonded through their carboxylic acid groups. The yellow circles represent Br, the red balls oxygen, the green areas carbon, and the white spheres hydrogen atoms. The alternating pattern seen in the STM image is also reproduced here. Further, as indicated by the parallelograms, the dimerized acid molecules occupy four rows of the graphite surface. (d) Molecular model representing the STM image of (b). Here, only *S*-enantiomers are depicted, and the black bars denote an *S-S* chiral pair. Again, the alternating Br-COOH-Br pattern is shown. Reprinted with permission from Leanna C. Giancarlo and George W. Flynn, Acc. Chem. Res. 2000, 33(7), 491-501. Copyright (2000) American Chemical Society.

Domains of opposite chirality were found not to contain any coadsorbed (*S*)-2-bromohexadecanoic acid.[23]

Note that in the absence of the achiral cosolute, 2-bromohexadecanoic acid forms a monolayer structure characterized by a different lamella-backbone angle (see Figure 14).[8] The formation of bromine dimers suggests that intermolecular interactions between bromine substituents play a role in driving this self-assembly.[8,24] Again, chiral micro-separation results, as inter-molecular interactions drive the formation of chirally pure, enantio-morphous domains, composed of a single type of chirally pure, hydrogen-bonded acid dimers.

Self-Assembly and Manipulation

Self-assembly on graphite has been probed for a wide variety of molecular species, some of which include functional groups that permit further, post-assembly manipulation. As an example, an STM image and corresponding model are shown in Figures 15a and 15b for an isophthalic acid derivative (ISA) self-assembled at the undecanol/graphite interface.[25,26] An ordered, lamellar structure is observed, with alternating rows of close-packed ISA and solvent (undecanol) molecules, stabilized by dispersion interactions (involving alkyl chains and the graphite substrate), electrostatic forces (involving the polar carboxylic acid groups and the semi-metallic graphite substrate), and hydrogen bonds (between the carboxylic acid and alcohol groups).

The isophthalic acid derivative under consideration belongs to the class of diacetylene compounds (R-C≡C-C≡C-R') where polymerization is known to occur in (three-dimensional) solid crystals upon exposure to ultraviolet radiation. High-resolution STM studies of ISA monolayers with submolecular resolution can address the question whether the UV-induced polymerization reaction also occurs in two dimensions. The STM images and proposed model shown in Figures 15a and 15b suggest that this might indeed be the case. As in three-dimensional crystals, the diacetylene (-C≡C-C≡C-) moieties of neighboring molecules are seen to occupy adjacent positions, presumably mimicking the transition state of the topochemical polymerization reaction. This is not the case for any additional ISA molecules present in the supernatant solution. Thus, it can be expected that UV irradiation will lead to selective polymerization of the interfacial layer only.

The results of UV illumination are shown in Figures 15c and 15d. The clear changes in STM image contrast suggest that the intermolecular polymerization reaction has taken place as anticipated.[25,26] Each individual lamella that used to consist of separate molecular entities has been transformed into a single conjugated polydiacetylene (=RC-C≡C-CR'=)n moiety with new mechanical and electronic properties. Due to their conjugated double and triple bonds, these molecularly thin "tapes" might serve as model systems for molecular wires.

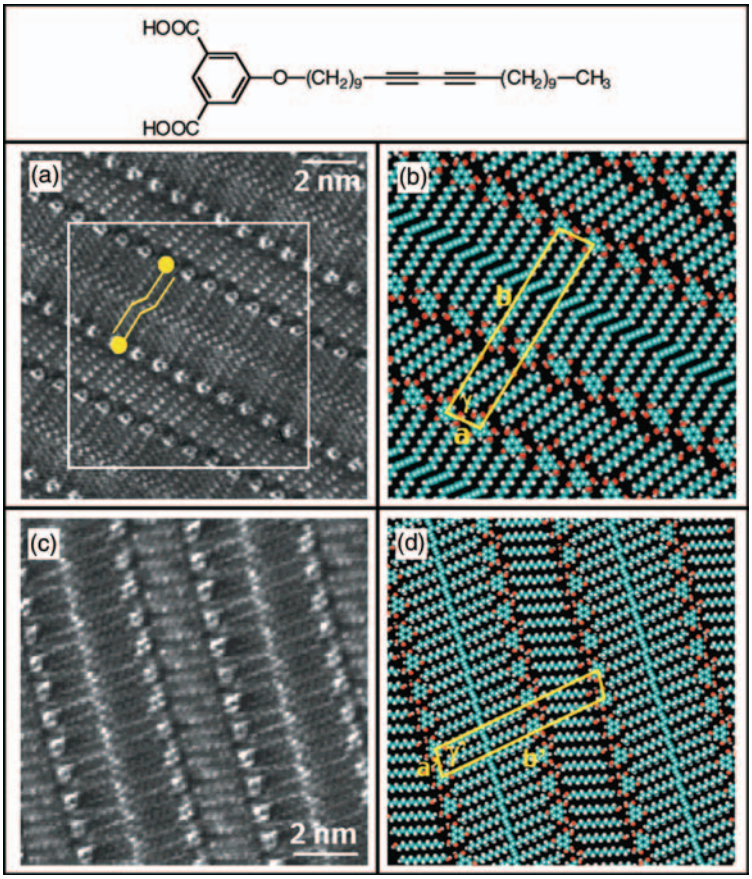

Figure 15. The isophthalic acid derivative under consideration (ISA) is shown in the top panel. (a) Constant height STM image (sample bias –1.2V, 1.0nA tunneling current) of a mixed ISA/undecanol monolayer formed at the undecanol/graphite interface before UV illumination. Yellow symbols highlight a pair of ISA molecules. (b) Proposed molecular model for the array of molecules included in the white box overlaid on the STM image shown in (a). (c) Constant height STM image (sample bias –0.5V, 1.0nA tunneling current) of ISA after UV illumination. (d) Proposed molecular model for the polymerized monolayer giving rise to the STM image shown in (c). Reprinted with permission from Steven de Feyter, Andre Gesquiere, Mohamed M. Abdel-Mottaleb, Petrus C. M. Grim, and Frans C. de Schryver, Acc. Chem. Res. 2000, 33(8), 520-31. Copyright (2000) American Chemical Society.

In general, post-assembly manipulation of interfacial monolayers can be induced through a variety of means. Aside from electromagnetic radiation, electrochemical control can be used to initiate chemical reactions. The application of brief voltage pulses through the STM tip can provide a means for highly localized nanoscale manipulation. As shown by Okawa et al.,[27,28] this strategy can be used successfully with dry monolayers of

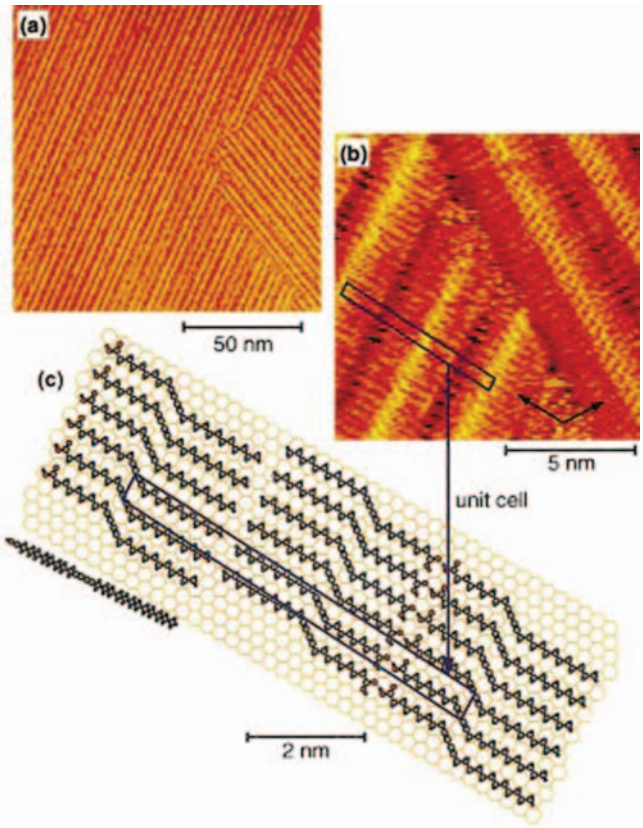

Figure 16. (a) Constant current STM image (sample bias −1.0V, 70pA tunneling current) of a 10,12-pentacosadiynoic acid monolayer at the air/graphite interface. (b) High-resolution STM image (sample bias +0.5V, 1.0nA tunneling current) emphasizing the packing structure. As indicated by the black arrows, the molecular axis is aligned with high symmetry axes of the underlying graphite substrate. (c) Proposed molecular model for the monolayer giving rise to the STM images displayed in (a) and (b). Black parallelograms shown in (b) and (c) depict a unit cell of the monolayer structure. Reprinted with permission from Y. Okawa and M. Aono, J. Chem. Phys. (2001), 115(5), 2317-22 (2001). Copyright (2001) by the American Institute of Physics.

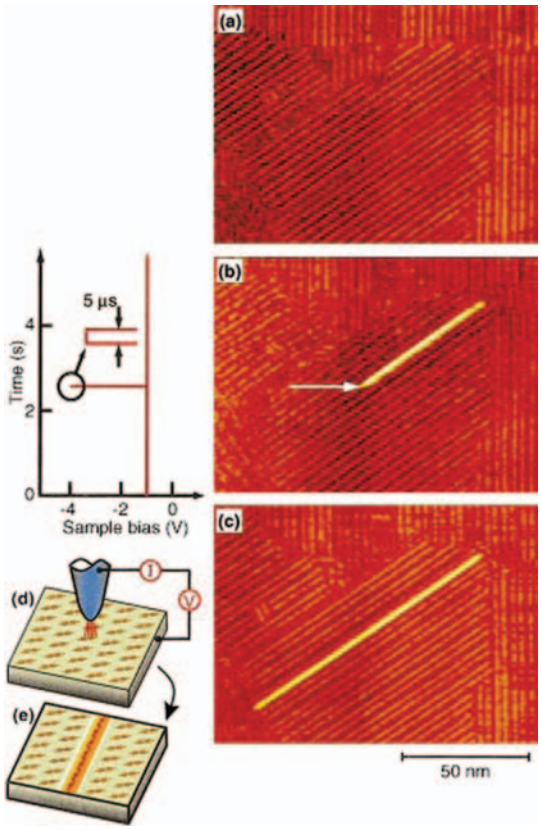

Figure 17. (a) Constant current STM image (sample bias −1.0V, 70pA tunneling current) of the original monomolecular layer of 10,12-pentacosadiynoic acid at the air/graphite interface. (b) Constant current STM image of the same area as in (a) but with application of a bias voltage pulse during imaging while the STM tip passed the location indicated by the white arrow. The image was acquired from the bottom to the top. The contrast of a single molecular row has changed drastically (c) Constant current STM image acquired immediately after the image shown in (b). The bright feature is seen to extend in both directions from the location where the voltage pulse was applied. (d), (e) Diagrams illustrating the initiation of chain polymerization with the STM tip. Reprinted with permission from Y. Okawa and M. Aono, J. Chem. Phys. (2001), 115(5), 2317-22 (2001). Copyright (2001) by the American Institute of Physics.

diacetylene derivatives self-assembled on graphite substrates. Figure 16 shows an STM image of a monolayer formed by 10,12-pentacosadiynoic acid (PCA) at the air/graphite interface.[27,28]

As in the previous example, the diacetylene derivative is found to form a monolayer structure that may be conducive to the topochemical polymerization reaction. Again, the diacetylene (-C≡C-C≡C-) moieties of neighboring molecules occupy adjacent positions with the required mutual orientation. The result of applying a brief voltage pulse through the STM tip is illustrated in Figure 17. A single row (~3nm wide) of individual PCA molecules has been transformed into a conjugated polydiacetylene, thus demonstrating the targeted creation of a molecular wire from self-assembled precursors. One could envision the utilization of such a process for the targeted interconnection of co-assembled molecular devices, model systems for which will be discussed in the next sections.

STM is seen to be a powerful tool not only for local probing but also for local nanoscale manipulation. Molecular self-assembly is often cited as an essential ingredient for future nanoscale engineering. These studies demonstrate a path for augmenting the power of self-assembly through targeted post-assembly manipulation.

Ring Systems and Electronic Structure

STM studies of self-assembly on graphite have not been limited to substituted alkanes. A wide range of molecular species has been interrogated, often containing a core of interest surrounded by alkyl tails and/or functional groups to facilitate self-assembly on graphite. Such investigations include an abundance of organic molecules with planar, extended, conjugated π-systems and moderate HOMO-LUMO gaps. In particular, numerous STM studies performed in UHV[29-32] as well as under ambient conditions[33,34] have focused on monolayers composed of porphyrins and phthalocyanines. Due to their interesting and easily tunable optical and electronic properties members of this versatile class of compounds are often considered candidates for model systems of molecular devices.

Figure 18 shows a high-resolution STM image of 21,23-Dihydro-5,10,15,20-tetrakis[4-(tetradecyloxy)phenyl] porphyrin (TTPP) at the air/graphite interface.[34] Clearly, an ordered monolayer structure is observed, presumably stabilized by the interdigitization of the 14-carbon long alkyl chains attached to each porphyrin. Consistent with this hypothesis, shorter chain analogs were found to produce less ordered monolayer structures.

The STM image shown in Figure 18 is clearly dominated by bright features. Their size and four-fold symmetry suggest that they arise from porphyrin cores that lie flat on the graphite substrate. The porphyrin cores are seen to be consistently brighter than the alkyl chains at their periphery as expected from the fact that the extended π-electron system of the porphyrin cores gives rise to occupied and unoccupied states that are much closer to the Fermi level than any electronic states with appreciable density on the alkyl chains.[7,11] UHV STM studies of porphyrins and phthalocyanines have additionally uncovered characteristic differences in submolecular image contrast depending on bias voltage polarity and metal atom substitution.[32,35,36]

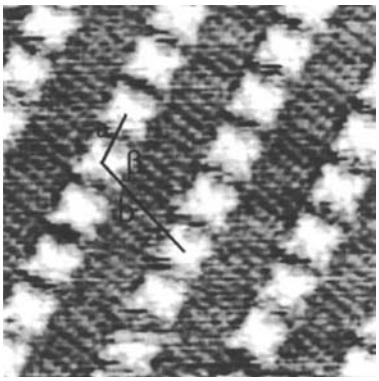

Figure 18. Constant current STM image (15nm×15nm, sample bias 0.752V, 1.032nA tunneling current) of 21,23-Dihydro-5,10,15,20-tetrakis[4-(tetradecyloxy)phenyl] porphyrin on graphite. The porphyrin cores appear as bright features of four-fold symmetry. Hongna Wang, Chen Wang, Qingdao Zeng, Shandong Xu, Shuxia Yin, Bo Xu, and Chunli Bai, Surf. Interface Anal. 2001; 32: 267. Copyright 2001 John Wiley and Sons Limited. Reprinted with permission.

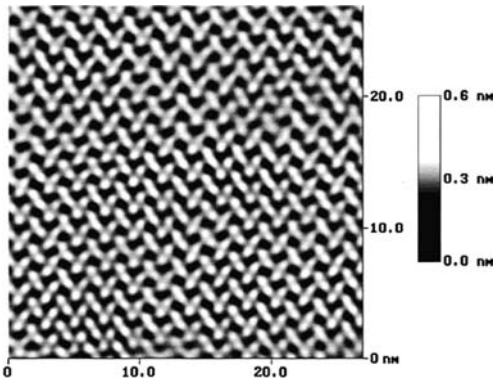

Figure 19. Constant current STM image (27nm×27nm, negative sample bias, 40pA tunneling current) of the 70° angled herringbone phase formed by bis(4-dibutylamino-2-hydroxyphenyl)squaraine adsorbed at the interface between a phenyloctane solution and the basal plane of graphite. Elongated bright features are assigned to the chromophores of individual molecules. Each feature appears slightly bisected, indicating enhanced tunneling over the phenyl rings as compared with the central squaraines unit. Reprinted with permission from M. E. Stawasz, D. L. Sampson, and B. A. Parkinson, Langmuir 2000, 16(5), 2326-42. Copyright (2000) American Chemical Society.

STM studies of planar ring-systems have been extended to include molecules consisting of several linked cyclic subunits. Figure 19 shows an STM image of a monolayer formed by bis(4-dibutylamino-2-hydroxyphenyl) squaraine.[37] While the image contrast does not reveal the exact configuration of the butyl chains, alkyl dispersion interactions presumably play a role in monolayer stabilization, as do interactions between the polar core groups. Depending on alkyl chain length a variety of self-assembled monolayer structures are observed.

As with the porphyrins discussed above, the bright contrast of the aromatic cores dominating the STM image displayed in Figure 19 may be attributed to electronic structure, rather than purely geometric effects. Electronic states near the Fermi level are likely to be localized at the aromatic ring system, rather than the insulating alkyl chains. Close inspection of Figure 19 reveals the elongated bright spots to be consistently bisected by a slight depression near their center. A simple consideration of electronic structure may explain this observed contrast within the aromatic core. In the symmetrically substituted squaraines under consideration, the phenyl groups are known to serve as electron donors while the central squaraine functions as electron acceptor. The donor-acceptor-donor structure of this compound leads to (aggregation-dependent) charge transfer behavior manifest in optical absorption bands. Giving up electrons most easily, the donor units must be where the highest occupied molecular orbital is localized. At negative sample bias, the HOMO (if sufficiently close to the Fermi level) may be expected to dominate electron tunneling. Indeed, the STM

image displayed in Figure 19 was acquired at negative sample polarity and the phenyl (donor) units appear as the brightest features.

Toward Molecular Electronics

Recently, STM studies have included large molecules specifically tailored both to facilitate self-assembly and for probing electron transport at the nanoscale in model systems for molecular electronics. Following early suggestions by Aviram and Ratner,[38] molecular analogs for current rectifiers (diodes) and transistors are being investigated where electron donor (D) and acceptors (A) units are linked covalently. STM constitutes an ideal tool for such studies, as the tunneling junction at the center of the STM technique intrinsically probes charge transport at the nanoscale. As illustrated in Figure 5 (see Section "Source of Image Contrast"), STM studies of molecules adsorbed on surfaces intrinsically address the mediation of charge transport by molecular states and their coupling to one of the electrodes (i.e., the conducting substrate supporting the molecule). Essentially the same diagram as shown in Figure 5 also applies for molecular conductance junctions (e.g., break or electro-migration junctions). However, STM provides the added advantage of (lateral) scanning, thus combining the spectroscopic mode with an imaging mode. In molecular conductance junctions, the presence of a molecule has to be inferred from the spectro-scopic data alone. The same is true for molecular orientation and bonding to the electrodes. In contrast, STM images can complement STS data acquired with a scanning tunneling microscope to ascertain the presence of the species of interest and determine its orientation and conformation. In addition, STS data can be acquired with the STM tip positioned over different parts of a given molecule, effectively mapping out the spatial variation of the conductance contributions associated with molecular orbitals.

Miura et al. have investigated a large, symmetric D-A-D system where oligo p-phenylene vinylene (OPV) donor units are attached to a perylenediimide (PDI) acceptor moiety (see Figure 20a).[39] The STM images displayed in Figures 20b, 20c, and 20e reveal the formation of ordered monolayer domains at the liquid-solid interface. Dispersion interactions between the alkyl chains attached to the D-A-D triad may play a role in stabilizing the self-assembled structure as suggested by the interdigitated dodecyloxy chains in the molecular model displayed in Figure 20d. The large molecular size and ordered monolayer structure observed in STM images permits the identification of donor and acceptor subunits (within individual molecules) so that their relative image contrast can be

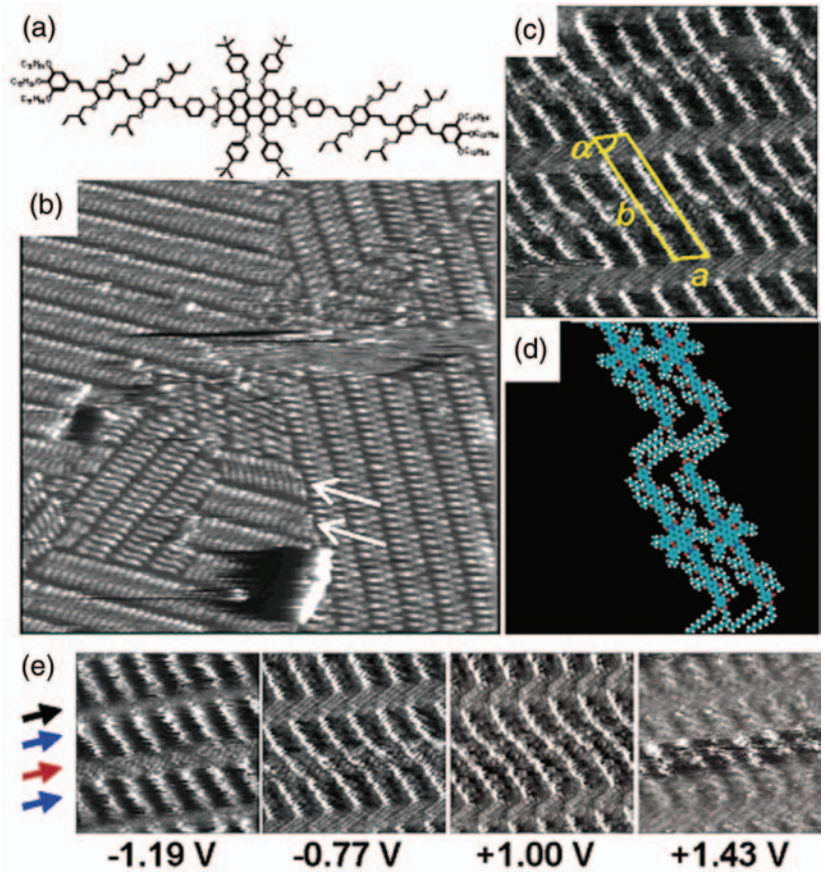

Figure 20. (a) Chemical structure of the D-A-D triad. (b) Constant height STM image (70.2nm × 70.2nm, sample bias –0.96V, 150pA tunneling current) of a D-A-D monolayer at the interface between a 1-phenyloctane solution and the basal plane of graphite. Arrows indicate mirror-image type packing. (c) High-resolution STM image (15.5nm × 15.5nm, sample bias –0.70V, 400pA tunneling current) with overlaid parallelogram indicating a monolayer unit cell. (d) Proposed molecular model reflecting the ordering in (c). (e) Bias-dependent imaging of the D-A-D triad (10.1nm × 10.1nm, 400pA tunneling current, sample bias indicated below each image). In order top-to-bottom, the arrows on the left refer to alkyl chains, donor units, acceptor units, and donor units. Reprinted with permission from Atsushi Miura, Zhijian Chen, Hiroshi Uji-i, Steven de Feyter, Magdalena Zdanowska, Pascal Jonkheijm, Albertus P. H. J. Schenning, E. W. Meijer, Frank Würthner, and Frans C. de Schryver, J. Am. Chem. Soc., 2003, 125(49), 14968-9. Copyright (2003) American Chemical Society.

examined as a function of bias voltage. Bias dependent imaging reveals brighter contrast (*i.e.*, higher tunneling current) for the donor moieties at negative sample bias, while the acceptor moieties are brighter at positive sample bias (see Figure 20e).

A simple physical picture has been proposed relating the observed bias dependent charge transmission to the electronic structure of the D-A-D system.[39] Absorption spectra indicate that the donor and acceptor moieties are electronically decoupled or weakly coupled, allowing frontier orbitals of the D-A-D triad to be assigned as belonging to individual subunits. As the electron donor units give up electrons most easily (by definition), the donor HOMO constitutes the highest filled state of the overall molecule and has a dominant influence on the surface LDOS just below the Fermi level. Thus, the OPV donor moieties support a higher tunneling current at negative sample bias, where filled surface states are being probed. Conversely, the LUMO of the PDI acceptor moiety dominates the density of empty surface states just above the Fermi level, making the PDI unit more transmissive at positive sample bias. Thus, the bias dependent charge transmission through this molecular device analog can be understood in terms of resonantly enhanced electron tunneling dominated by individual electronic states associated with molecular subunits.[39]

Recent STM studies of model systems for molecular devices also include a prototypical single-molecule chemical-field-effect transistor where nanometer-sized charge transfer complexes control current rectification through a covalently-linked ring system.[40] At the center of these investigations is an electron-rich hexa-peri-hexabenzocoronene (HBC) core, surrounded by six electron-poor anthraquinone (AQ) subunits.[40] As in the previous example, individual molecular subunits can be identified in high-resolution STM images and the bias polarity dependent tunneling probability can be understood in terms of resonantly enhanced electron tunneling. Upon adding the electron-rich 9,10-dimethoxyanthracene (DMA) to the solution, DMA-AQ charge-transfer (CT) complexes are formed. New self-assembled domains that incorporate CT complexes are found to coexist with remaining domains free of DMA. As a local, high-resolution probe, STM allows the separate interrogation of individual molecules in these coexisting self-assembled structures. Current-voltage curves obtained atop the HBC cores are found to be asymmetric (rectifying) with the degree of asymmetry controlled by the presence (or absence) of the DMA-AQ-CT complex. The interfacial dipole associated with formation of the CT complex causes a relative shift between the adsorbate's electronic states and the Fermi level of the substrate.[40] Thus, STM has been used to probe the charge transmission through a single molecule and its control by a chemically-induced electric field effect.

The STM studies discussed in this section have combined self-assembly on graphite with detailed single-molecule conductance measurements by using specifically tailored molecules synthesized prior to deposition on the graphite substrate. Other examples discussed in this application note include the post-assembly modification of self-assembled monolayers (*e.g.*, topochemical polymerization of diacetylene derivatives)[25,27,28] on graphite. Furthermore, self-assembled monolayers of substituted alkanes on graphite have been used as templates for organizing nanoparticles.[41] Based on combinations of these ingredients one could envision powerful recipes for the targeted creation and interrogation of complex model systems for molecular devices with STM playing a central role.

Summary and Conclusions

What sets STM apart from other SPMs is the use of the tunneling current between tip and sample as error signal for the SPM feedback loop. While this feature limits STM studies to sufficiently conductive samples, the steep exponential distance dependence of the tunneling current allows for a spatial resolution rarely achieved in other SPM modes. At the same time, the ability to perform STM work in air, under solutions, and within electrochemical cells has made the interrogation of self-assembly practical. Veeco SPMs have played a prominent role in this endeavor with numerous STM studies addressing the structure and dynamics of self-assembled monolayers in exquisite detail.

Aside from the controlled bottom-up (self) assembly at interfaces, important ingredients envisioned for future nanoscale engineering include single-molecule devices. The understanding and control of charge transport in model systems for such molecular devices constitutes an important focal point of current efforts in nanoscience. Due to its ability to interrogate the mediation of charge transport by individual molecular states, STM is uniquely positioned as an important tool in this area. Applications discussed in the present note include recent STM studies that have been designed to interrogate charge transport in molecular devices while building on previous work to self-assemble the species of interest into ordered arrays. Future studies can be envisioned where the power of this approach is augmented further through combination with post-assembly modification and co-assembly of multiple nanoscale components, thus allowing STM to play an even more important role in nanoscience.

Bibliography

1. Binning, G.; Rohrer, H.; Gerber, C.; Weibel, E. Tunneling through a controllable vacuum gap. App. Phys. Lett. 1982, 40 178-180.
2. Binning, G.; Rohrer, H.; Gerber, C.; Weibel, E. Surface studies by scanning tunneling microscopy. Phys. Rev. Lett. 1982, 49 57-61.
3. Binning, G.; Rohrer, H.; Gerber, C.; Weibel, E. *7x7* reconstruction on Si(111) resolved in real space. Phys. Rev. Lett. 1983, 50 120-123.
4. Rohrer, H. Scanning tunneling microscopy. Proc. Natl. Acad. Sci. U. S. A. 1987, 84 (14), 4666.
5. Tersoff, J.; Hamann, D. R. Theory and application for the scanning tunneling microscope. Phys. Rev. Lett. 1983, 50 (25), 1998-2001.
6. Tersoff, J.; Hamann, D. R. Theory of the scanning tunneling microscope. Phys. Rev. B 1985, 31 (2), 805-813.
7. Giancarlo, L. C.; Flynn, G. W. Scanning tunneling and atomic force microscopy probes of self-assembled, physisorbed monolayers: peeking at the peaks. Annu. Rev. Phys. Chem. 1998, 49 297-336.
8. Giancarlo, L. C.; Flynn, G. W. Raising flags: applications of chemical marker groups to study self-assembly, chirality, and orientation of interfacial films by scanning tunneling microscopy. Acc. Chem. Res. 2000, 33 (7), 491-501.
9. Poirier, G. E. Characterization of organosulfur molecular monolayers on Au(111) using scanning tunneling microscopy. Chem. Rev. 1997, 97 (4), 1117-1127.
10. Magonov, S. N.; Whangbo, M. H. Surface analysis with STM and AFM: experimental and theoretical aspects of image analysis; VCH: Weinheim, New York, 1996.
11. Claypool, C. L.; Faglioni, F.; Goddard, W. A., III; Gray, H. B.; Lewis, N. S.; Marcus, R. A. Source of image contrast in STM images of functionalized alkanes on graphite: a systematic functional group approach. J. Phys. Chem. B 1997, 101 (31), 5978-5995.
12. Eigler, D. M.; Weiss, P. S.; Schweizer, E. K. Imaging Xe with a low-temperature scanning tunneling microscope. Phys. Rev. Lett. 1991, 66 (9), 1189-1192.
13. Liang, W.; Whangbo, M. H.; Wawkuschewski, A.; Cantow, H. J.; Magonov, S. N. Electronic origin of scanning tunneling microscopy images and carbon skeleton orientations of normal alkanes adsorbed on graphite. Adv. Mater. 1993, 5 (11), 817-821.
14. Fang, H.; Giancarlo, L. C.; Flynn, G. W. Identification of the conformation of individual molecules by scanning tunneling microscopy. J. Phys. Chem. B 1999, 103 (27), 5712-5715.
15. Ho, W. Single-molecule chemistry. J. Chem. Phys. 2002, 117 (24), 11033-11061.
16. Li, L. Y.; Chen, S. F.; Jiang, S. Y. Molecular-scale mixed alkanethiol monolayers of different terminal groups on Au(111) by low-current scanning tunneling microscopy. Langmuir 2003, 19 (8), 3266-3271.
17. Rabe, J. P.; Buchholz, S. Commensurability and mobility in 2-dimensional molecular patterns on graphite. Science 1991, 253 (5018), 424-427.
18. Herwig, K. W.; Matthies, B.; Taub, H. Solvent effects on the monolayer structure of long n-alkane molecules adsorbed on graphite. Phys. Rev. Lett. 1995, 75 (17), 3154-3157.
19. Askadskaya, L.; Rabe, J. P. Anisotropic molecular dynamics in the vicinity of order-disorder transitions in organic monolayers. Phys. Rev. Lett. 1992, 69 (9), 1395-1398.
20. Fang, H.; Giancarlo, L. C.; Flynn, G. W. Packing of Br(CH2)10COOH and Br(CH2)11COOH on graphite: an odd-even length effect observed by scanning tunneling microscopy. J. Phys. Chem. B 1998, 102 (38), 7421-7424.
21. Hibino, M.; Sunni, A.; Tsuchiya, H.; Hatta, I. Microscopic origin of the odd-even effect in monolayer of fatty acids formed on a graphite surface by scanning tunneling microscopy. J. Phys. Chem. B 1998, 102 (23), 4544-4547.
22. De Feyter, S.; Grim, P. C. M.; Rucker, M.; Vanoppen, P.; Meiners, C.; Sieffert, M.; Valiyaveettil, S.; Mullen, K.; De Schryver, F. C. Expression of chirality by achiral coadsorbed molecules in chiral monolayers observed by STM. Angew. Chem. Intl. Ed. Engl. 1998, 37 (9), 1223-1226.
23. Yablon, D. G.; Giancarlo, L. C.; Flynn, G. W. Manipulating self-assembly with achiral molecules: an STM study of chiral segregation by achiral adsorbates. J. Phys. Chem. B 2000, 104 (32), 7627-7635.

24. Fang, H.; Giancarlo, L. C.; Flynn, G. W. Direct determination of the chirality of organic molecules by scanning tunneling microscopy. J. Phys. Chem. 1998, 102 7311-7315.
25. Grim, P. C. M.; De Feyter, S.; Gesquiere, A.; Vanoppen, P.; Rucker, M.; Valiyaveettil, S.; Moessner, G.; Mullen, K.; De Schryver, F. C. Submolecularly resolved polymerization of diacetylene molecules on the graphite surface observed with scanning tunneling microscopy. Angew. Chem. Intl. Ed. Engl. 1997, 36 (23), 2601-2603.
26. De Feyter, S.; Gesquiere, A.; Abdel-Mottaleb, M. M. S.; Grim, P. C. M.; De Schryver, F. C. Scanning tunneling microscopy: a unique tool in the study of chirality, dynamics, and reactivity in physisorbed organic monolayers. Acc. Chem. Res. 2000, 33 (8), 520-531.
27. Okawa, Y.; Aono, M. Linear chain polymerization initiated by a scanning tunneling microscope tip at designated positions. J. Chem. Phys. 2001, 115 (5), 2317-2322.
28. Okawa, Y.; Aono, M. Nanoscale control of chain polymerization. Nature 2001, 409 (6821), 683-684.
29. Hipps, K. W.; Barlow, D. E.; Mazur, U. Orbital mediated tunneling in vanadyl phthalocyanine observed in both tunnel diode and STM environments. J. Phys. Chem. B 2000, 104 (11), 2444-2447.
30. Scudiero, L.; Barlow, D. E.; Mazur, U.; Hipps, K. W. Scanning tunneling microscopy, orbital-mediated tunneling spectroscopy, and ultraviolet photoelectron spectroscopy of metal(II) tetraphenylporphyrins deposited from vapor. J. Am. Chem. Soc. 2001, 123 (17), 4073-4080.
31. Hipps, K. W.; Scudiero, L.; Barlow, D. E.; Cooke Jr., M. P. A self-organized 2-dimensional bifunctional structure formed by supramolecular design. J. Am. Chem. Soc. 2002, 124 (10), 2126-2127.
32. Lackinger, M.; Müller, T.; Gopakumar, T. G.; Müller, F.; Hietschold, M.; Flynn, G. W. Tunneling voltage polarity dependent submolecular contrast of naphthalocyanine on graphite. A STM study of close-packed monolayers under ultrahigh-vacuum conditions. J. Phys. Chem. B 2004, 108 (7), 2279-2284.
33. Qiu, X.; Wang, C.; Zeng, Q.; Xu, B.; Yin, S.; Wang, H.; Xu, S.; Bai, C. L. Alkane-assisted adsorption and assembly of phthalocyanines and porphyrins. J. Am. Chem. Soc. 2000, 122 (23), 5550-5556.
34. Wang, H.; Wang, C.; Zeng, Q.; Xu, S.; Yin, S.; Xu, B.; Bai, C. L. Chain-length-adjusted assembly of substituted porphyrins on graphite. Surf. Interface Anal. 2001, 32 266-270.
35. Lu, X.; Hipps, K. W.; Wang, X. D.; Mazur, U. Scanning tunneling microscopy of metal phthalocyanines: d7 and d9 cases. J. Am. Chem. Soc. 1996, 118 (30), 7197-7202.
36. Lu, X.; Hipps, K. W. Scanning tunneling microscopy of metal phthalocyanines: d6 and d8 cases. J. Phys. Chem. B 1997, 101 (27), 5391-5396.
37. Stawasz, M. E.; Sampson, D. L.; Parkinson, B. A. Scanning tunneling microscopy investigation of the ordered structures of dialkylamino hydroxylated squaraines adsorbed on highly oriented pyrolytic graphite. Langmuir 2000, 16 2326-2342.
38. Aviram, A.; Ratner, M. A. Molecular rectifiers. Chem. Phys. Lett. 1974, 29 (2), 277-283.
39. Miura, A.; Chen, Z.; Hiroshi, U.; De Feyter, S.; Zdanowska, M.; Jonkheijm, P.; Schenning, A. P. H. J.; Meijer, E. W.; Würthner, F.; De Schryver, F. C. Bias-dependent visualization of electron donor (D) and electron acceptor (A) moieties in a chiral DAD triad molecule. J. Am. Chem. Soc. 2003, 125 (49), 14968-14969.
40. Jäckel, F.; Watson, M. D.; Müllen, K.; Rabe, J. P. Prototypical single-molecule chemical-field-effect transistor with nanometer-sized gates. Phys. Rev. Lett. 2004, 92 (18), 188303.
41. Hoeppener, S.; Chi, L.; Fuchs, H. Formation of Au55 strands on a molecular template at the solid-liquid interface. Nano Letters 2002, 2 (5), 459-463.

Veeco Instruments Inc.
112 Robin Hill Road
Santa Barbara, CA 93117
805-967-1400 • 1-888-24-VEECO
www.veeco.com

Solutions for a nanoscale world.™

AN85, Rev A0, 1/05